THE JOURNAL OF PHYSICAL CHEMISTRY B
A JOURNAL OF THE AMERICAN CHEMICAL SOCIETY

pubs.acs.org/JPCB
Article

Oscillatory Motion of a Camphor Disk on a Water Phase with an Ionic Liquid Sensitive to Transition Metal Ions

Hua Er,* Yukang Bai, Muneyuki Matsuo, and Satoshi Nakata*

Cite This: J. Phys. Chem. B 2025, 129, 592−597
Read Online

ABSTRACT: We investigated oscillatory motion of a camphor disk floating on water containing 5 mM hexylethylenediaminium trifluoroacetate (HHexen-TFA) as an ionic liquid (IL). The frequency of the oscillatory motion increased with increasing concentrations of the transition metal ions Cu^{2+} and Ni^{2+} but was insensitive to Na^{+}, Ca^{2+}, and Mg^{2+}, the typical metal ions in the water phase. The surface tension of the water phase containing 5 mM HHexen-TFA also increased with increasing concentrations of Cu^{2+} and Ni^{2+} but was insensitive to Na^{+}, Ca^{2+}, and Mg^{2+}. Based on density functional theory, metal-ion species-dependent frequency response is discussed with regard to surface tension as the force of self-propulsion and complex formation between HHexen-TFA and metal ions. These results suggest that complex formation between the transition metal ions (Cu^{2+}, Ni^{2+}) and the ethylenediamine group in the IL increases the surface tension around the camphor disk, resulting in an increase in the frequency of oscillatory motion with increasing concentrations of Cu^{2+} or Ni^{2+}. The present study suggests that the nature of self-propulsion can be created by complexation, which changes the force of self-propulsion.

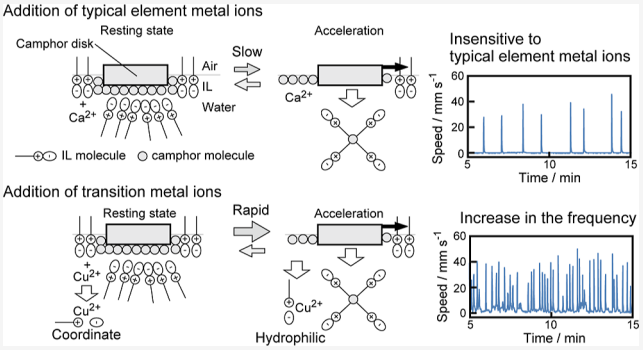

1. INTRODUCTION

Development of inanimate self-propelled objects has been investigated to carry matter in a micrometer or millimeter space.[1−6] Self-propelled objects are mainly classified into two types based on the driving force of their motion. One driving force is electrophoresis or bubbles produced on noble metals, such as Pt nanorods and Au Janus particles.[7−16] The other is the spatial gradient in interfacial tension around an amphiphilic object.[17−25] Most inanimate self-propelled objects move randomly or unidirectionally depending on the intrinsic or extrinsic cause, and the direction and speed of motion are determined by the inhomogeneity of the internal or external field, for example, the shape of the object or the electromagnetic field.[11,25−28] In contrast, animate self-propulsion, such as bacterial motion, can characteristically change the nature of motion while responding to their physicochemical environments.[29] The introduction of nonlinear properties, such as oscillation and pattern formation, into inanimate self-propelled systems is one strategy to enhance the autonomy of the systems because characteristic features of motion can be created based on physicochemical nonlinearity.[22−25,30−33]

On the other hand, ionic liquids (ILs), composed of both cationic and anionic parts, have been studied as electrolytes or solvents.[34,35] ILs can potentially introduce physicochemically controllable nonlinearity into inanimate self-propulsion owing to their characteristic solubility and cation-sensitive coordination ability, which depend on their polar groups and alkyl chain length.[35−39] We previously reported a self-propelled camphor pill or boat on water or surfactant aqueous solutions such as sodium dodecyl sulfate (SDS).[25,32] Recently, we found that the nature of camphor disk motion could be changed by the addition of the ionic liquids hexylethylenediaminium trifluoroacetate (HHexen-TFA) and hexylammonium trifluoroacetate (HHexam-TFA) in water.[40] That is, bifurcation of self-propulsion among uniform motion, repetition between rest and motion, and no motion was observed depending on the IL concentration.

In this study, a camphor disk exhibited oscillatory motion between rest and motion on an aqueous solution of HHexen-TFA (see Scheme 1). The features of the oscillatory motion were sensitive to transition metal ions; that is, the frequency of

Scheme 1. Chemical Structure of the Ionic Liquid HHexen-TFA Used in the Present Article

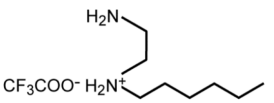

Received: October 28, 2024
Revised: December 18, 2024
Accepted: December 19, 2024
Published: December 26, 2024

https://doi.org/10.1021/acs.jpcb.4c07310
J. Phys. Chem. B 2025, 129, 592−597

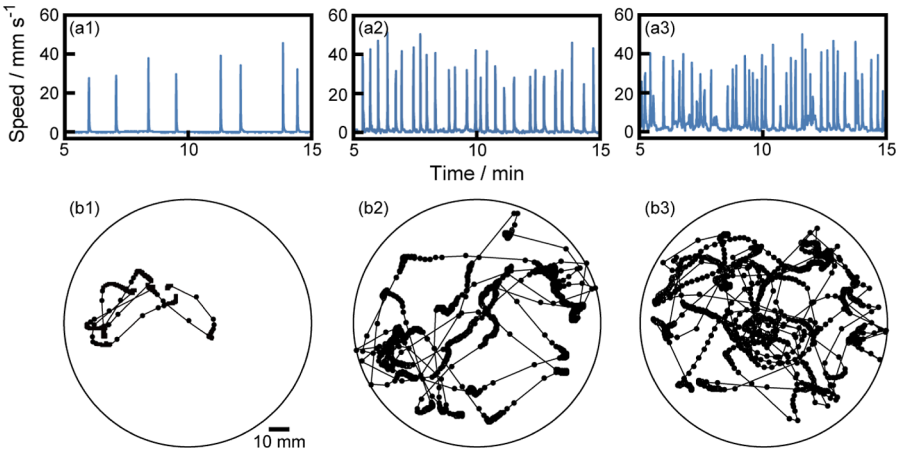

Figure 1. (a) Temporal change of the speed for camphor motion and (b) trajectories of the center position of a camphor disk on 5 mM HHexen-TFA aqueous solution for different concentrations of $CuCl_2$ [(1) 0, (2) 2, and (3) 5 mM] from t = 5 to 15 min (top view). The time interval of motion was 1/30 s. The circle in (b) corresponds to the Petri dish. The movies of motion in (1), (2), and (3) are provided in the Supporting Information as Movies S1, S2, and S3, respectively.

the oscillatory motion increased with increasing concentrations of Cu^{2+} and Ni^{2+} added to the IL aqueous phase. In contrast, the frequency of the oscillatory motion was not sensitive to Na^+, Ca^{2+}, and Mg^{2+}, which are typical metal ions. Different responses in the frequency of the oscillatory motion depending on the metal ion species are discussed regarding the surface tension and complex formation between HHexen-TFA and the metal ion species. The present study suggests that the features of the oscillatory motion can be altered by the interfacial properties of the complex formed with the IL, depending on the metal ion species.

2. EXPERIMENTAL SECTION

The purity of HHexen-TFA ($C_{10}H_{21}N_2O_2F_3$), as illustrated in Scheme 1,[37,38] was evaluated using ^{13}C NMR measurement on Bruker 400 MHz spectrometer and CHN elemental analysis on GmbH Vario EL instrument. (+)-Camphor ($C_{10}H_{16}O$, with a purity >96%) was supplied by Shanghai Macklin. A camphor disk characterized by a diameter of 6.0 mm, thickness of 1.0 mm, and a mass of approximately 30 mg, was prepared according to the previous study.[25,32] The disk was delicately positioned to float on a 40 mL, 4 mm deep aqueous solution containing HHexen-TFA, which was contained within a glass Petri dish featuring an inner diameter of 120 mm and a depth of 15 mm. Ultrapure water was produced on a water purification machine manufactured by Ningbo Dansboton Environmental Protection Tech. Co., Ltd., China. The experiments were performed at least three times under each experimental condition to ascertain the reproducibility of obtained phenomena. The motion of the camphor disk was meticulously observed and recorded using an Olympus STYLUS XZ-2 model digital video camera (minimum time resolution: 1/30 s) in an air-conditioned room maintained at 298 ± 2 K. The self-propelled movement of the object was subsequently analyzed using ImageJ software, provided by the National Institutes of Health in the United States. Additionally, the surface tension at the air/aqueous interface of an aqueous solution containing HHexen-TFA was precisely measured using a BZY-2 model surface tensiometer manufactured by Shanghai Heng Ping Instrument Factory.

The intermolecular interaction energy between the IL and metal chloride (molar ratio: 1:1) was numerically calculated based on density functional theory (DFT) with M06-2X functional and 6-311G(d,p) basis set using the Gaussian 09 W software package.[41] The optimized configurations of the IL–metal chlorides ($CuCl_2$, $NiCl_2$, $MgCl_2$, and $CaCl_2$) are described in the Supporting Information.

3. RESULTS

First, we monitored the self-propulsion of a camphor disk on a 5 mM HHexen-TFA aqueous phase at different concentrations of $CuCl_2$, as shown in Figure 1. Oscillatory motion between rest and motion was observed for 5 mM HHexen-TFA in the absence of $CuCl_2$ [Figure 1(1)]. The frequency of the oscillatory motion increased with increasing concentration of $CuCl_2$ [Figure 1(2),(3)]. The trajectories of the oscillatory motion were random for 0, 2, and 5 mM $CuCl_2$. The maximum speed of the oscillatory motion was almost independent of the concentration of $CuCl_2$. The variations in the speed and trajectory of the oscillatory motion of 5 mM HHexen-TFA with the addition of $CaCl_2$ are shown in Figure S1 of the Supporting Information.

Figure 2 shows the frequency of the oscillatory motion of a camphor disk depending on the concentration of the metal chlorides, $CuCl_2$ (empty circles), $NiCl_2$ (empty squares), $CaCl_2$ (filled squares), $MgCl_2$ (filled triangles), and NaCl (filled circles), C_{mc}, in a 5 mM HHexen-TFA aqueous solution. The

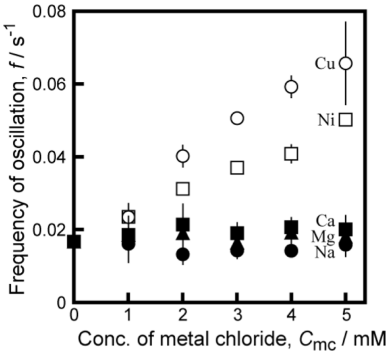

Figure 2. Frequency of oscillatory motion depending on the concentration of metal chlorides (NaCl, $CaCl_2$, $MgCl_2$, $CuCl_2$, $NiCl_2$), C_{mc}, in a 5 mM HHexen-TFA aqueous solution. Error bars represent standard deviation.

https://doi.org/10.1021/acs.jpcb.4c07310
J. Phys. Chem. B 2025, 129, 592−597

frequency of the oscillatory motion increased with increasing concentrations of $CuCl_2$ and $NiCl_2$. In contrast, the frequency did not change with the concentrations of $CaCl_2$, $MgCl_2$, or NaCl. The amplitude of the oscillatory motion was almost independent of the metal chloride concentration used in this study (see Figure S2 on the amplitude of oscillatory motion in the Supporting Information).

Measurement of the surface tension of the aqueous phase is significant to elucidate the mechanism by which the frequency of oscillatory motion is sensitive to $CuCl_2$ and $NiCl_2$ because the force of camphor self-propulsion depends on the spatial difference in the surface tension around it on the aqueous surface.[25] Figure 3a shows the surface tension (γ) of the 5 mM

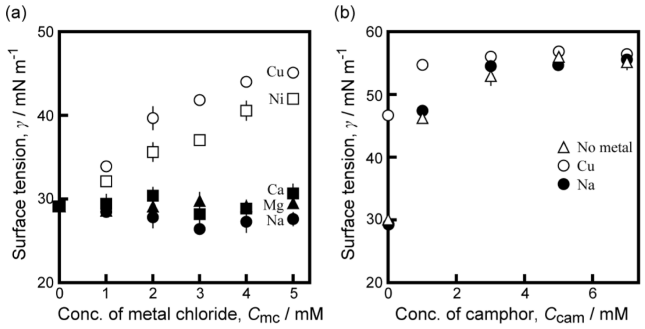

Figure 3. Surface tension depending on the concentration of (a) metal chloride, NaCl (filled circles), $CaCl_2$ (filled squares), $MgCl_2$ (filled triangles), $CuCl_2$ (empty circles), $NiCl_2$ (empty squares)), C_{mc}, in a 5 mM HHexen-TFA aqueous solution and (b) camphor, C_{cam}, in a 5 mM HHexen-TFA aqueous solution with 5 mM metal chloride (NaCl (filled circles), $CuCl_2$ (empty circles) or without metal chloride (empty triangles). Error bars represent standard deviation.

HHexen-TFA aqueous phase depending on C_{mc} for $CuCl_2$, $NiCl_2$, $CaCl_2$, $MgCl_2$, and NaCl. γ increased with increasing concentrations of $CuCl_2$ and $NiCl_2$. In contrast, γ was not sensitive to $CaCl_2$, $MgCl_2$, and NaCl. Figure 3b shows γ of the 5 mM HHexen-TFA aqueous phase with or without 5 mM $CuCl_2$ or NaCl, depending on the concentration of camphor, C_{cam}. γ was increased with C_{cam}. γ for $CuCl_2$ was higher than that for NaCl or without metal chloride at $C_{cam} \leq 3$ mM, but was similar at $C_{cam} \geq 5$ mM.

To investigate the coordination of metal ions with the ethylenediamine group and TFA in the IL, we calculated the interaction energies between the IL and metal chlorides. The configurations of one ethylenediamine in IL−one metal chloride ($MgCl_2$, $CaCl_2$, $NiCl_2$, or $CuCl_2$) complex were individually optimized at the M06-2X/6-311G(d,p) level using DFT calculations, as illustrated in Figures S3 of the Supporting Information. The basis set superposition error (BSSE) and zero-point vibrational energy (ZPVE)-corrected intermolecular interaction energies (ΔE_0^{BSSE}/kJ mol^{-1}) for the optimized configurations involving coordination with ethylenediaminium in the IL for different metal ions are presented in Table 1. The ΔE_0^{BSSE} for Ni^{2+} and Cu^{2+} were more negative than those for Mg^{2+} and Ca^{2+}. The configurations of one TFA in IL−one metal chloride ($MgCl_2$, $CaCl_2$, $NiCl_2$, or $CuCl_2$) complex are shown in Figure S4 of the Supporting Information. Regarding the stability of the coordination with TFA and metal ions, similar values of ΔE_0^{BSSE} were obtained for Mg^{2+}, Ca^{2+}, Ni^{2+}, and Cu^{2+} (see the right side of Table 1).

Table 1. Intermolecular Interaction Energy, ΔE_0^{BSSE} (kJ mol^{-1}), of the Optimized Configurations for the IL-Metal Chloride (Coordinated with Cation Ethylenediamine (Left Side) and Anion TFA (Right Side))

metal ions	ΔE_0^{BSSE}/kJ mol^{-1} (coordinated with cation ethylenediamine)	ΔE_0^{BSSE}/kJ mol^{-1}(coordinated with anion TFA)
Mg^{2+}	−28	−41
Ca^{2+}	−26	−41
Ni^{2+}	−42	−38
Cu^{2+}	−43	−39

4. DISCUSSION

Based on the present results and previous works,[22−25,34−40,42−44] we discuss the increase in the frequency of the oscillatory motion of a camphor disk floating in a 5 mM HHexen-TFA aqueous phase with the addition of $CuCl_2$ and $NiCl_2$. The force of camphor self-propulsion is due to the surface tension difference around the disk as a one-dimensional system; that is, $\Delta\gamma = \gamma_{cL} - \gamma_{cR}$, where γ_{cL} and γ_{cR} are the surface tensions on the left and right edges of the camphor disk, respectively.[25] On the water phase without HHexen-TFA and metal ions, the camphor disk continuously supplies camphor molecules onto the water surface, resulting in continuous motion. If the camphor disk moves continuously, the surface tension difference remains due to the sublimation and dissolution of camphor molecules from the water surface into the air and water phase, respectively, and continuous motion is maintained.[25]

In contrast, the oscillatory motion observed for 5 mM HHexen-TFA (see Figures 1 and S1) suggests that the camphor disk alternately gains and loses the force of self-propulsion, as schematically indicated in Figure 4. We previously reported the mechanism of the oscillatory motion of the camphor disk in 5 mM HHexen-TFA.[40] The surface tension γ for the saturated aqueous solution of camphor (~55 mN m^{-1} at ~7 mM) is higher than that for 5 mM HHexen-TFA without camphor (~30 mN m^{-1}). Therefore, the camphor disk remains at rest because the water surface is covered by a layer of HHexen-TFA molecules (see the left side of Figure 4a). However, the surface tension is increased by the addition of camphor (see Figure 3b) since camphor molecules are distributed on the water surface in the place of HHexen-TFA, and the mixture of HHexen-TFA and camphor is dissolved into the water phase. As a result, the camphor disk can accelerate toward regions of lower HHexen-TFA concentration, that is, higher surface tension (right side of Figure 4a). When the camphor disk moves to another location with a higher HHexen-TFA concentration, it stops again because the state around the camphor disk returns to the resting state. Thus, the oscillatory motion is repeated between resting at regions of higher HHexen-TFA concentration and acceleration due to surface tension changes resulting from the mixture of HHexen-TFA and camphor (Figure 4a).

Figure 3a suggests that the HHexen-TFA molecular layer is desorbed from the air/water interface into the bulk phase with the addition of $CuCl_2$ or $NiCl_2$, as indicated at the left side of Figure 4b. This occurs because HHexen-TFA coordinates with Cu^{2+} or Ni^{2+},[42−44] and the water-soluble HHexen-TFA-Cu^{2+} or HHexen-TFA-Ni^{2+} complex dissolve into the water phase. Table 1 suggests that the coordination of the ethylenediamine group in HHexen-TFA to transition metal ions (Ni^{2+} and Cu^{2+}) has an important role in the frequency of the oscillatory motion. As the resting time decreases, the frequency of the oscillatory motion increases with increasing concentration of $CuCl_2$ or $NiCl_2$. In

https://doi.org/10.1021/acs.jpcb.4c07310
J. Phys. Chem. B 2025, 129, 592−597

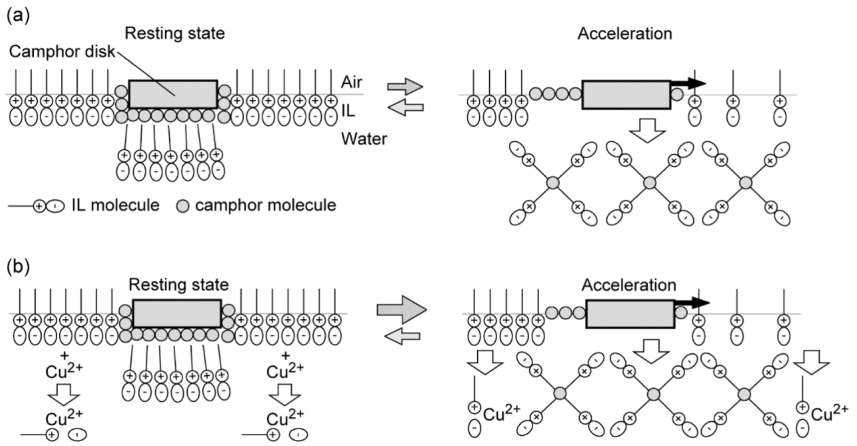

Figure 4. Schematic representation of the mechanism of oscillatory motion of a camphor disk placed on an HHexen-TFA aqueous phase: (a) without metal chloride and (b) with $CuCl_2$ (side view).

contrast, the frequency of the oscillatory motion is independent of the addition of NaCl, $CaCl_2$, and $MgCl_2$ because the surface tension is independent of their concentrations (see Figure 3a). Moreover, the surface tension dependence on C_{cam} without metal chloride is similar to that for 5 mM NaCl (see Figure 3b). These results suggest that it is difficult to form water-soluble complexes with Na^+, Ca^{2+}, or Mg^{2+}.

The differences in the frequency responses of the oscillatory motion between the transition metal ions (Cu^{2+}, Ni^{2+}) and the typical metal ions (Na^+, Ca^{2+}, and Mg^{2+}) (see Figures 1, S1, S2, and 2) may be due to the stability of the complex between HHexen-TFA and the cation species, especially the stability of the complex between the ethylenediamine group and Cu^{2+} or Ni^{2+}. This is consistent with the fact that the stability constants (log K) for the transition metal ions are higher than those of typical main group metal ions—for example, for ethylenediamine:[45] Ca^{2+}, 0.20; Mg^{2+}, 0.37; Ni^{2+}, 6.98; and Cu^{2+}, 10.06—which agrees with the experimental results in the present study.

Table 1 shows the differences in the HHexen-TFA complexes with various metal ions (Cu^{2+}, Ni^{2+}, Mg^{2+}, and Ca^{2+}), as verified by DFT calculations. The optimized structure of camphor coordinated with HHexen-TFA is shown in Figure S5 of the Supporting Information. That is, the coordination stabilities of the ethylenediamine group in HHexen-TFA with Cu^{2+} and Ni^{2+} ($\Delta E_0^{BSSE} \sim -42$ kJ mol^{-1}) are higher than those with Mg^{2+} and Ca^{2+}($\Delta E_0^{BSSE} \sim -27$ kJ mol^{-1}) (left side of Table 1). However, the coordination stabilities between TFA and the metal ions (Mg^{2+}, Ca^{2+}, Ni^{2+}, and Cu^{2+}) are similar (right side of Table 1). In other words, the coordination stability between the ethylenediamine group and Cu^{2+} or Ni^{2+} induces characteristic features of motion depending on the concentration.

5. CONCLUSIONS

In this study, we found oscillatory motion of a camphor disk which preferred dwelling at a certain location before switching its direction of motion, like run-and-tumble motion of bacteria. The frequency of the oscillatory motion of a camphor disk on water with HHexen-TFA was found to increase with the addition of Cu^{2+} and Ni^{2+} as transition metal ions but was insensitive to Na^+, Ca^{2+}, and Mg^{2+} as typical metal ions. We discussed the increase in the frequency of the oscillatory motion with increasing concentrations of Cu^{2+} and Ni^{2+} regarding the dependence of the surface tension on concentrations of metal chlorides and camphor. The solubility of the complex composed of HHexen-TFA and the divalent cations of transition elements, such as Cu^{2+} and Ni^{2+}, plays an important role in increasing the frequency of the oscillatory motion. The effect of anions should be considered to understand the characteristic motion of a camphor disk on the ionic liquid aqueous phase with the addition of metal salt in the future work. The present study suggests that the inanimate nature of self-propulsion driven by the difference in surface tension can be designed by tuning the chemical and physical characteristics of the IL, such as its ability to form complexes with divalent cations. In other words, the metal cation species can be detected based on the features of the oscillatory motion of the camphor disk through coordination with the IL.

■ ASSOCIATED CONTENT

Supporting Information

The Supporting Information is available free of charge at https://pubs.acs.org/doi/10.1021/acs.jpcb.4c07310.

The detail of DFT calculation; Time-variation of the speed and trajectory of motion for a camphor disk on a 5 mM HHexen-TFA aqueous solution at 2 and 5 mM $CaCl_2$; Amplitude of oscillatory motion of a camphor disk depending on the concentration of metal chloride in a 5 mM HHexen-TFA aqueous solution; Optimized configurations of ethylenediaminium in IL coordinated with metal chlorides; Optimized configurations of TFA in IL coordinated with metal chlorides; Optimized configuration of IL coordinated with camphor (PDF)

Movie S1 corresponds to Figure 1(1) (AVI)

Movie S2 corresponds to Figure 1(2) (AVI)

Movie S3 corresponds to Figure 1(3) (AVI)

■ AUTHOR INFORMATION

Corresponding Authors

Hua Er − *School of Chemistry and Chemical Engineering, Ningxia Key Laboratory of Solar Chemical Conversion Technology, Key Laboratory for Chemical Engineering and Technology, State Ethnic Affairs Commission, North Minzu University, Yinchuan 750021, P. R. China;* orcid.org/0000-0001-7353-0174; Email: huaer0101@hotmail.com

Satoshi Nakata − *Graduate School of Integrated Sciences for Life, Hiroshima University, Higashi-Hiroshima 739-8526 Hiroshima, Japan;* orcid.org/0000-0002-7290-1508;

Phone: +81-82-424-7409; Email: nakatas@hiroshima-u.ac.jp

Authors

Yukang Bai − *School of Chemistry and Chemical Engineering, Ningxia Key Laboratory of Solar Chemical Conversion Technology, Key Laboratory for Chemical Engineering and Technology, State Ethnic Affairs Commission, North Minzu University, Yinchuan 750021, P. R. China;* orcid.org/0009-0002-8202-2782

Muneyuki Matsuo − *Graduate School of Integrated Sciences for Life, Hiroshima University, Higashi-Hiroshima 739-8526 Hiroshima, Japan; Graduate School of Arts and Sciences, The University of Tokyo, Tokyo 153-8902, Japan;* orcid.org/0000-0002-2559-3522

Complete contact information is available at: https://pubs.acs.org/10.1021/acs.jpcb.4c07310

Author Contributions

H. E. contributed to the planning of examination and writing and editing the draft. Y. B. contributed to the examination and analysis of the data, and editing the draft. M. M. contributed to discussion, review and editing the draft. S. N. contributed to planning of the research, writing, and reviewing the draft.

Notes

The authors declare no competing financial interest.

■ ACKNOWLEDGMENTS

The present study was supported by the Key Project at North Minzu University (Project no. 2023ZRLG 23) to H.E., JSPS KAKENHI (grant nos. JP20H02712, 24K22324, JP21H00996), the Cooperative Research Program of "Network Joint Research Center for Materials and Devices" (no. 20241009), and Iketani Science and Technology Foundation (0351181-A) to S.N., and MEXT Leading Initiative for Excellent Young Researchers (JPMXS0320230007) to M.M. We also gratefully acknowledge the joint master's student program involving supervision from both China and abroad.

■ REFERENCES

(1) Soto, F.; Karshalev, E.; Zhang, F.; Esteban Fernandez de Avila, B. E. F. E.; Nourhani, A.; Wang, J. Smart Materials for Microrobots. *Chem. Rev.* **2022**, *122*, 5365−5403.
(2) Dwivedi, P.; Pillai, D.; Mangal, R. Self-Propelled Swimming Droplets. *Curr. Opin. Colloid Interface Sci.* **2022**, *61*, 101614.
(3) Xu, Y.; Bian, Q.; Wang, R.; Gao, J. Micro/Nanorobots for Precise Drug Delivery via Targeted Transport and Triggered Release: A Review. *Int. J. Pharm.* **2022**, *616*, 121551.
(4) Zhou, H.; Mayorga-Martinez, C. C.; Pané, S.; Zhang, L.; Pumera, M. Magnetically Driven Micro and Nanorobots. *Chem. Rev.* **2021**, *121*, 4999−5041.
(5) Yang, Z.; Snyder, D.; Sathyan, A.; Balazs, A.; Emrick, T. Smart Droplets Stabilized by Designer Surfactants: From Biomimicry to Active Motion to Materials Healing. *Adv. Funct. Mater.* **2023**, *33*, 2306819.
(6) Kumar, P.; Zhang, Y.; Ebbens, S. J.; Zhao, X. 3D Inkjet Printed Self-Propelled Motors for Micro-Stirring. *J. Colloid Interface Sci.* **2022**, *623*, 96−108.
(7) Si, Z. T.; Wu, Z.; He, W.; He, Q. Self-Propelled Predator-Prey of Swarming Janus Micromotors. *iScience* **2023**, *26*, 106112.
(8) Raman, H.; Das, S.; Sharma, H.; Singh, K.; Gupta, S.; Mangal, R. Dynamics of Active SiO_2−Pt Janus Colloids in Dilute Poly-(Ethyleneoxide) Solutions. *ACS Phys. Chem. Au* **2023**, *3*, 279−2899.
(9) Arqué, X.; Patiño, T.; Sánchez, S. Enzyme-Powered Micro- and Nano-Motors: Key Parameters for an Application-Oriented Design. *Chem. Sci.* **2022**, *13*, 9128−9146.
(10) Wang, Q.; Steinbock, O. Shape-Preserving Conversion of Calcium Carbonate Tubes to Self-Propelled Micromotors. *Phys. Chem. Chem. Phys.* **2022**, *24*, 14538−14544.
(11) Salinas, G.; Tieriekhov, K.; Garrigue, P.; Sojic, N.; Bouffier, L.; Kuhn, A. Lorentz Force-Driven Autonomous Janus Swimmers. *J. Am. Chem. Soc.* **2021**, *143*, 12708−12714.
(12) Liu, R.; Zhao, L.; Yang, S.; Lin, J.; Wang, X.; Chen, D.; Lu, G.; Chen, H.; Wang, Z.; Ye, Z.; Lu, J. Self-Propelled Micro-/Nanomotors of ZnO Nanoshuttles Induced by Surface Defects. *J. Phys. Chem. C* **2023**, *127*, 12026−12034.
(13) Wu, Y.; Si, T.; Gao, C.; Yang, M.; He, Q. Bubble-Pair Propelled Colloidal Kayaker. *J. Am. Chem. Soc.* **2018**, *140*, 11902−11905.
(14) Dey, K. K.; Sen, A. Chemically Propelled Molecules and Machines. *J. Am. Chem. Soc.* **2017**, *139*, 7666−7676.
(15) Mayol, B.; Pradana-López, S.; García, A.; de la Torre, C.; Díez, P.; Villalonga, A.; Anillo, C.; Vilela, D.; Sánchez, A.; Martínez-Ruiz, P.; Martínez-Máñez, R.; Villalonga, R. Self-Propelled Enzyme-Controlled IR-Mesoporous Silica Janus Nanomotor for Smart Delivery. *J. Colloid Interface Sci.* **2024**, *671*, 294−302.
(16) Liu, J.; Li, J.; Wang, G.; Yang, W.; Yang, J.; Liu, Y. Bioinspired Zeolitic Imidazolate Framework (ZIF-8) Magnetic Micromotors for Highly Efficient Removal of Organic Pollutants from Water. *J. Colloid Interface Sci.* **2019**, *555*, 234−244.
(17) Fujino, T.; Matsuo, M.; Pimienta, V.; Nakata, S. Oscillatory Motion of an Organic Droplet Reflecting a Reaction Scheme. *J. Phys. Chem. Lett.* **2023**, *14*, 9279−9284.
(18) Bala, M.; Singh, V. Surface Tension Gradient Driven Autonomous Fatty Acid-Tetrahydrofuran Liquid Moving Drops: Spreading to Pinning. *J. Mol. Liq.* **2023**, *375*, 121361.
(19) Zahorán, R.; Kumar, P.; Horváth, D.; Tóth, Á. Self-Propulsion of a Calcium Alginate Surfer. *Soft Matter* **2023**, *19*, 8033−8039.
(20) Kitahata, H.; Koyano, Y.; Löffler, R. J.; Górecki, J. Complexity and Bifurcations in the Motion of a Self-Propelled Rectangle Confined in a Circular Water Chamber. *Phys. Chem. Chem. Phys.* **2022**, *24*, 20326−20335.
(21) Xu, Y.; Kang, J.; Sun, M.; Shan, J.; Guo, W.; Zhang, Q. Insights into Characteristic Motions and Negative Chemotaxis of the Inanimate Motor Sensitive to Sodium Chloride. *J. Colloid Interface Sci.* **2024**, *660*, 953−960.
(22) Nakata, S.; Nagayama, M.; Kitahata, H.; Suematsu, N. J.; Hasegawa, T. Physicochemical Design and Analysis of Self-Propelled Objects that Are Characteristically Sensitive to Environments. *Phys. Chem. Chem. Phys.* **2015**, *17*, 10326−10338.
(23) Suematsu, N. J.; Nakata, S. Evolution of self-propelled objects: From the Viewpoint of Nonlinear Science. *Chem.—Eur. J.* **2018**, *24*, 6308−6324.
(24) Huang, H.-J.; Nuthalapati, K.; Sheng, Y.-J.; Tsao, H.-K. Precursor Film of Self-Propelled Droplets: Inducing Motion of a Static Droplet. *J. Mol. Liq.* **2022**, *368*, 120729.
(25) *Self-Organized Motion: Physicochemical Design Based on Nonlinear Dynamics*; Nakata, S.; Pimienta, V.; Lagzi, I.; Kitahata, H.; Suematsu, N. J., Eds.; The Royal Society of Chemistry: Cambridge, 2019.
(26) Holló, G.; Suematsu, N. J.; Ginder, E.; Lagzi, I. Electric Field Assisted Motion of a Mercury Droplet. *Sci. Rep.* **2021**, *11*, 2753.
(27) You, M.; Chen, C.; Xu, L.; Mou, F.; Guan, J. Intelligent Micro/Nanomotors with Taxis. *Acc. Chem. Res.* **2018**, *51*, 3006−3014.
(28) Song, J.; Shklyaev, O. E.; Sapre, A.; Balazs, A. C.; Sen, A. Self-Propelling Macroscale Sheets Powered by Enzyme Pumps. *Angew. Chem., Int. Ed.* **2024**, *63*, No. e202311556.
(29) Jarrell, K. F.; McBride, M. J. The Surprisingly Diverse Ways that Prokaryotes Move. *Nat. Rev. Microbiol.* **2008**, *6*, 466−476.
(30) Thakur, S.; Chen, J. X.; Kapral, R. Interaction of a Chemically Propelled Nanomotor with a Chemical Wave. *Angew. Chem., Int. Ed. Engl.* **2011**, *50*, 10165−10169.
(31) Suematsu, N. J.; Mori, Y.; Amemiya, T.; Nakata, S. Spontaneous Mode Switching of Self-Propelled Droplet Motion Induced by a Clock

Reaction in the Belousov−Zhabotinsky Medium. *J. Phys. Chem. Lett.* **2021**, *12*, 7526−7530.
(32) Xu, Y.; Takayama, N.; Er, H.; Nakata, S. Oscillatory Motion of a Camphor Object on a Surfactant Solution. *J. Phys. Chem. B* **2021**, *125*, 1674−1679.
(33) Fujita, R.; Matsuo, M.; Nakata, S. Self-Propelled Object that Generates a Boundary with Amphiphiles at an Air/Aqueous Interface. *J. Colloid Interface Sci.* **2024**, *663*, 329−335.
(34) Ruan, Q. Q.; Yao, M.; Yuan, D.; Dong, H.; Liu, J.; Yuan, X.; Fang, W.; Zhao, G.; Zhang, H. Ionic Liquid Crystal Electrolytes: Fundamental, Applications and Prospects. *Nano Energy* **2023**, *106*, 108087.
(35) Krishnan, A.; Gopinath, K. P.; Vo, D.-V. N.; Malolan, R.; Nagarajan, V. M.; Arun, J. Ionic Liquids, Deep Eutectic Solvents and Liquid Polymers as Green Solvents in Carbon Capture Technologies: A Review. *Environ. Chem. Lett.* **2020**, *18*, 2031−2054.
(36) Buettner, C. S.; Cognigni, A.; Schröder, C.; Bica-Schröder, K. Surface-Active Ionic Liquids: A review. *J. Mol. Liq.* **2022**, *347*, 118160.
(37) Er, H.; Wang, H. Properties of Protic Ionic Liquids Composed of N-Alkyl (= Hexyl, Octyl and 2-Ethylhexyl) Ethylenediaminum Cations with Trifluoromethanesulfonate and Trifluoroacetate Anion. *J. Mol. Liq.* **2016**, *220*, 649−656.
(38) Er, H.; Xu, Y.; Zhao, H. Properties of Monoprotic Ionic Liquids Composed of Hexylammonium and Hexylethylenediaminium Cations with Trifluoroacetate and Bis (Trifluoromethylsulfonyl) Imide Anions. *J. Mol. Liq.* **2019**, *276*, 379−384.
(39) Wang, C.; Zhu, J. J.; Qiu, Y.; Wang, H.; Xu, Y.; Haghani, H.; Er, H. Protic Ionic Liquids with Chelating Amine. *J. Solution Chem.* **2024**.
(40) Hua, E.; Gao, J.; Xu, Y.; Matsuo, M.; Nakata, S. Self-Propelled Motion Controlled by Ionic Liquids. *Phys. Chem. Chem. Phys.* **2024**, *26*, 8488−8493.
(41) Frisch, M. J.; et al. *Gaussian 09*. revision D.01; Gaussian, Inc.: Wallingford CT, 2013.
(42) Watanabe, M.; Nakayama, C.; Yasuda, H.; Harada, M.; Iida, M. Interactions of Nickel(II) Ions in Protic Ionic Liquids Comprising *N*-Hexyl(or *N*-2-Ethtylhexyl)Ethylenediamines. *J. Mol. Liq.* **2016**, *214*, 77−85.
(43) Takemura, S.; Kawakami, S.; Harada, M.; Iida, M. Solvation Structure of a Copper(II) Ion in Protic Ionic Liquids Comprising *N*-Hexylethylenediamine. *Inorg. Chem.* **2014**, *53*, 9667−9678.
(44) Watanabe, M.; Takemura, S.; Kawakami, S.; Syouno, E.; Kurosu, H.; Harada, M.; Iida, M. Sites of Protonation and Copper(II)-Complexation in Protic Ionic Liquids Comprised of *N*-Hexylethylenediaminium Cation. *J. Mol. Liq.* **2013**, *183*, 50−58.
(45) Burgess, D. R. *NIST SRD 46. Critically Selected Stability Constants of Metal Complexes*. version 8.0 for Windows; National Institute of Standards and Technology, 2004.

https://doi.org/10.1021/acs.jpcb.4c07310
J. Phys. Chem. B 2025, 129, 592−597